Environmental Science & Technology

pubs.acs.org/est

Article

Chemistry and Isotope Fractionation of Divalent Mercury during Aqueous Reduction Mediated by Selected Oxygenated Organic Ligands

Huifang Zhao, Bo Meng,* Guangyi Sun, Che-Jen Lin, Xinbin Feng,* and Jonas Sommar*

Cite This: *Environ. Sci. Technol.* 2021, 55, 13376−13386

Read Online

ACCESS | Metrics & More | Article Recommendations | Supporting Information

ABSTRACT: We have investigated the chemistry and Hg isotope fractionation during the aqueous reduction of Hg^{II} by oxalic acid, *p*-quinone, quinol, and anthraquinone-2,6-disulfonate (AQDS), a derivate of anthraquinone (AQ) that is found in secondary organic aerosols (SOA) and building blocks of natural organic matter (NOM). Each reaction was examined for the effects of light, pH, and dissolved O_2. Using an excess of ligand, UVB photolysis of Hg^{II} was seen to follow pseudo-first-order kinetics, with the highest rate of $\sim 10^{-3}$ s^{-1} observed for AQDS and oxalic acid. Mass-dependent fractionation (MDF) occurs by the normal kinetic isotope effect (KIE). Only the oxalate ion, rather than oxalic acid, is photoreactive when present in HgC_2O_4, which decomposes via two separate pathways distinguishable by isotope anomalies. Upon UVB photolysis, only the reduction mediated by AQDS results in a large odd number mass-independent fractionation (odd-MIF) signified by enrichment of odd isotopes in the reactant. Consistent with the rate, MDF, and odd-MIF reported for fulvic acid, our AQDS result confirms previous assumptions that quinones control Hg^{II} reduction in NOM-rich waters. Given the magnitude of odd-MIF triggered via a radical pair mechanism and the significant rate in the presence of air, reduction of Hg^{II} by photoproducts of AQDS may help explain the positive odd-MIF observed in ambient aerosols depleted of Hg^{II}.

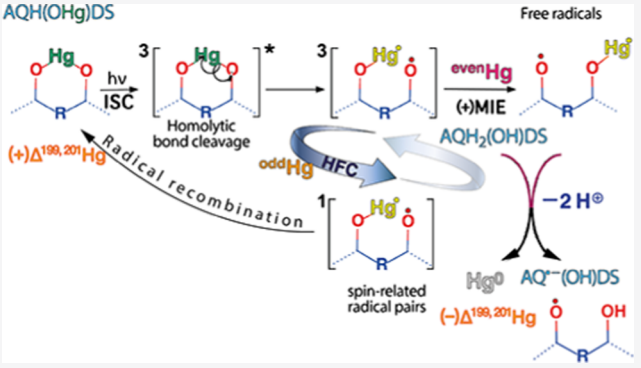

KEYWORDS: *Hg, isotope fractionation, UV radiation, reduction, aqueous phase*

INTRODUCTION

Globally, anthropogenic Hg emissions to the atmosphere and its subsequent deposition have increased the storage of this neurotoxic element in land, water, and air. Hg has been designated as a top-priority toxic chemical by international agencies and is now regulated by the legally binding Minamata Convention (UNEP-MC).[1] Evaluation of the efficacy of reductions in emissions set by the UNEP-MC critically depends on the knowledge of the dynamics of the global Hg cycle. Of these processes, the effects of redox reactions, methylation−demethylation, and the exchange of gaseous mercury between air and natural ecosystems are still uncertain.[2]

The advent of stable Hg isotope composition measurement in nature has established that the photo-initiated reduction of Hg^{II} is omnipresent and important in the environment.[3] In surface waters and atmospheric hydrometeors, the photo-induced reduction is particularly important, although the detailed mechanisms are not well understood. In both media types, Hg^{II} complexation and interaction with natural organic matter (NOM) play a pivotal role in Hg speciation and mobility.[4,5] The chemical reducing effect of dissolved NOM (humic substances) on Hg^{II} has been recognized for nearly 50 years.[6] In addition to macromolecular ligands, classes of abundant low-molecular-weight organic compounds (LMWOCs) that display a high Henry's law constant and strong complexation of Hg^{II} and include labile moieties towards oxidation (e.g., being decarboxylated) or chromophores are viable candidates to efficiently reduce Hg^{II} in the aqueous phase.[7,8] Examples are oxygenated compounds such as dicarboxylic acids, dicarbonyls, and quinones produced via atmospheric oxidation over several reaction cycles of a more volatile precursor molecule ("chemical aging"), which can be either biogenic or anthropogenic (to take an example, C_2H_2/C_2H_4 for $(COOH)_2$[9]). They are major constituents of secondary organic aerosols (SOA), which represents a major component of the fine-particle fraction of aerosols that has profound effects on the global climate and human health.[10]

Received: May 18, 2021
Published: September 14, 2021

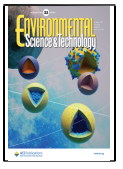

https://doi.org/10.1021/acs.est.1c03171
Environ. Sci. Technol. 2021, 55, 13376−13386

They are also building blocks of NOM and can serve as proxies for NOM with varying structural and functional properties. In NOM, quinone/hydroquinone (Q/QH_2) pairs are important redox-active moieties acting as both electron acceptors and donors in the oxidation−reduction cycle. Zheng et al.[11] inferred that reduced NOM-quinones account for most Hg^{II} reduction in anoxic environments, while Hg^0 oxidation is induced by thiols (forming Hg^{II}−NOM complexes via ligand-induced oxidative complexation).[12,13] Since the study of Zheng et al.[11] was based on experiments with reduced NOM, a study of simpler chemical systems with free Q/QH_2 molecules serves to elucidate the mechanism at the molecular level. To our knowledge, the reduction of Hg^{II} by QH_2 has not been investigated in detail, although it is known that *p*-quinol can reduce mercuric species to Hg^0.[14] Berkovic et al.[15] noted that *p*-naphthoquinone (NQ) is a very poor reductant of Hg^{II} relative to the $CO_2^{\bullet-}$ radical formed by photosensitized degradation of formic acid.

The aqueous reduction of Hg^{II} complexes may include primary (intramolecular) processes with charge transfer and secondary (intermolecular) reactions caused by reactive intermediates. Photo- or thermolabile Hg^{II} complexes are characterized by low-energy ligand-to-metal charge transfer (LMCT) excited states inclined to cause internal redox processes resulting in oxidation of a ligand and reduction of the divalent Hg ion.[16] In this study, we investigate two types of organic ligands that can act as both one- (1e) and two-electron (2e) reducing agents, namely QH_2 and oxalate. Although photochemical oxidation of oxalate to CO_2 is a characteristic feature of its transition metal complexes, there is a shift from a 1e-step radical-type mechanism involving lighter metal ions (e.g., Fe^{II}/Fe^{III} and $Co^{II}/^{III}$) to an internal 2e-redox process that dominates for some second- and third-row metal ions.[17] For example, the photochemistry of $\{Fe(C_2O_4)_3\}^{3-}$ follows a rapid 1e-LMCT step succeeded by the oxidized oxalate ion ($C_2O_4^{\bullet-}$) dissociating into free CO_2 and $CO_2^{\bullet-}$, which in turn reduces another $\{Fe(C_2O_4)_3\}^{3-}$ to Fe^{II} in a secondary reaction.[18] For second- and third-row transition metal ions that are relatively stable when complexed in low-oxidation states that differ by two units (e.g., $Re^{I/III}$, $Rh^{I/III}$, $Ir^{I/III}$, $Pd^{0/II}$, $Pt^{0/II}$), photochemical metal-oxalate reductive elimination via ligand fragmentation has been documented.[17,19] Thus, 2e-LMCT occurs here photoinduced as part of a concerted series of electron rearrangements (heterolytic breaking of σ-bonds in the complex), resulting in the oxalate ligand being eliminated as two molecules of CO_2 and the oxidation number of the metal ion decreasing by two units. This mechanism occurs without discernible intermediates such as free radicals.[20] Thus, for reduction mechanism studies, it is required to clarify whether the reaction occurs through 1e- and/or 2e reductions. As aforementioned, no light is required for QH_2 to reduce the aquatic mercuric ion to Hg^0, but it remains uncertain if the mechanism is intramolecular 2e transfer as it is for the environmentally relevant $Hg^{2+} + SO_3^{2-}$ reaction occurring in the dark.[21]

Concerning the prospects of anomalous Hg isotope fractionation in water, the primary process is 1e-LMCT, which by homolytic bond rapture produces radical pairs with spins that are either parallel (triplet) or antiparallel (singlet). The following spin mixing may trigger a large magnitude of odd number mass-independent fractionation (odd-MIF) (magnetic isotope effect, MIE). Homolysis of Hg^{II} molecules with polar bonds (e.g., $HgCl_2$) can lead to either positive (odd isotopes are enriched in the reactant) or negative (odd isotopes are depleted in the reactant) MIE depending on the reaction conditions.[22] Secondary reduction by free radicals as well as photolytic and thermal reductive elimination may give odd-MIF on a smaller scale by the nuclear volume effect (NVE).[23] In addition to quenching of triplet complex states, the presence of dissolved O_2 causes radicals such as $Hg^{\bullet+}$ produced by the 1e-LMCT mechanism to be scavenged with reoxidation to Hg^{2+} as a result. In terrestrial surface waters, besides photoreduction of Hg^{II}, the photodissociation of organic Hg^{II} (CH_3-Hg^+ species) contributes substantially to produce significant positive odd-MIF[22] in the reservoir. Conversely, in the atmosphere with insignificant background levels of CH_3-Hg^+, a more positive $\Delta^{199}Hg^{II}$ in SOA[24,25] compared to primary particles[26,27] should relate to the photoreduction of Hg^{II}.

Here, the kinetics and isotope fractionation during aqueous Hg^{II} reduction are presented for a series of selected oxygenated organic ligands. The kinetics of one of the reductions has been studied previously,[7,8,28] but the present study includes a more comprehensive study that systematically assesses the effect of light spectrum, pH, and dissolved O_2. For all ligands, we examine the reaction mechanism at the molecular level, which has seldomly been done in the past literature.

EXPERIMENTAL SECTION

Materials. The following organic ligands were investigated: oxalic acid ($H_2C_2O_4/(COOH)_2$), *p*-quinone (BQ), quinol (BQH_2), and anthraquinone-2,6-disulfonate (AQDS). Further details regarding the chemicals and reagents used in this study are tabulated and described in the Supporting Information (Materials section).

Method—Reduction Experiments. A 1000 ± 5 mg L^{-1} Hg^{II} stock solution was made by dissolving HgO in diluted (1%) $HClO_4$. As diluted Hg^{II} solutions undergo losses during storage due to, e.g., wall reactions,[29] all working solutions were freshly prepared for each experimental session by dilution of the original stock solution. The specific LMWOC was dissolved in 300 mL of Milli-Q water, which in turn was spiked with an Hg^{II} aliquot to yield an initial total Hg^{2+} concentration of ∼1 μM. LMWOCs were always present in excess with a default of 300 stoichiometric equivalents to one Hg^{II}. The initial pH of the Hg^{II}−LMWOC solutions at ∼3.6 was adjusted to the desired pH by the addition of either diluted $HClO_4$ or NaOH. By using ClO_4^- as counterion, interfering photodecomposition (NO_3^-)[30] or complexation (Cl^-)[8] is prevented. Production of Hg^0 in blanks was generally negligible over the experimental time (Figure S1). The reaction mixtures intended for photolytic experiments were after preparation left in the dark (wrapped in Al foil) for at least 1 h, allowing for equilibration to occur. A set of 500 mL Pyrex reaction vessels with gastight caps was used in the experiments, which were conducted in a temperature-controlled cabinet (295 ± 1 K) equipped with a light bank that may alternatively hold two either UVB or UVA compact fluorescent lights (model PL-S 9W/10/2P and PL-S 9W/ 01/ 2P, Phillips). The spectral power distribution of light transmitted into the reaction vessel was in each photoexperiment measured with a handheld spectroradiometer (model OHSP-350UV, Hopoocolor Ltd., Hangzhou, China). Photon fluxes in the reaction vessel were typically ∼2×10^{15} and ∼6×10^{14} cm^{-2} s^{-1} during the UVA and UVB experiments, respectively (Table S1). We have examined that the Hg in

https://doi.org/10.1021/acs.est.1c03171
Environ. Sci. Technol. 2021, 55, 13376−13386

the light sources had natural isotopic compositions (Table S2). Immediately before an experiment, depending on whether oxic or anoxic conditions were desired, the initial Hg^{II}−LMWOC solution was purged with O_2 mixtures in Ar/high-purity Ar to saturate or deplete the solution of O_2, respectively. This procedure also removed any initial trace of Hg^0. At regular intervals, the irradiated solution was first stripped from dissolved Hg^0 and subsequently, a subsample (∼10 mL) of the remaining Hg^{II} (aq) was withdrawn from the bottom of the reaction vessel. An optimized purging rate of 150 mL min^{-1} was deployed, yielding a carryover of 99.3 ± 0.6% for Hg^0 after 20 min of bubbling (Figure S2). For the assessment of the kinetics, the amounts of Hg^{II} and Hg^0 were measured by dual-stage Au amalgamation and cold-vapor atomic fluorescence spectroscopy,[31] while for the determination of Hg isotopic ratios, the purged Hg^0 from the solution was quantitatively oxidized and trapped (101.4 ± 4.5%, n = 6, Figure S2) in reversed aqua regia (40%) before analysis by cold-vapor multi-collector inductively coupled plasma mass spectrometry (CV-MC-ICP-MS). Depending on LMWOC reactivity, the total irradiation time deployed ranged from 1 to 6 h. The speciation of Hg^{II} in various experiments was estimated using thermodynamic modeling software (Spana[32] and ChemEQL;[33] see Figure S3 and Table S5).

Mass Balance. The recovery efficiencies of Hg^{II} and the product Hg^0 were evaluated for the intermittent isotopic sample by comparing the loaded Hg^{II} mass and stipulated f_r in the reaction mixture with that of the remaining reactant Hg^{II} withdrawn for analysis (f_R), the product Hg^0 purged and trapped into an oxidizing solution (f_P), and products retrieved from wall deposits (f_W). The latter portion of Hg was found to be <0.1% of the initial Hg and was considered negligible. In Table S3, the mass balance of Hg (%) is given for each organic reactant as the sum of f_R and f_P. In general, the mass balances were near unity, with the exception of the AQDS experiments, which demonstrate a relatively low recovery of 86.0 ± 1.1%.

Isotope Composition Measurements. Hg isotopic ratios were determined by a Nu-Plasma II CV-MC-ICP-MS (Nu Instruments Ltd., U.K.). The sample introduction system consists of a continuous-flow cold-vapor generation system (model HGX-200, CETAC Corp.) coupled to an Apex-Q desolvation unit (Elemental Scientific Inc.) for Hg and Tl introduction, respectively. $SnCl_2$ was used as the reducing agent and mixed online with Hg standards or samples to generate Hg^0. The Hg^0 vapor from the CV generation system was mixed with a dry Tl aerosol produced via the desolvation device.

Following Blum and Bergquist,[34] we report our results as

$$\delta^{xxx}\mathrm{Hg}\ (‰) = \left[\left(\frac{^{xxx}\mathrm{Hg}}{^{198}\mathrm{Hg}}\right)_{\mathrm{sample}} / \left(\frac{^{xxx}\mathrm{Hg}}{^{198}\mathrm{Hg}}\right)_{\mathrm{NIST\ 3133}} - 1\right] \times 1000$$

to describe the mass dependent fractionation (MDF), and $\Delta^{xxx}\mathrm{Hg} = \delta^{xxx}\mathrm{Hg} - \delta^{202}\mathrm{Hg}\cdot\beta_{xxx}$, where β_{xxx} is 0.252 for ^{199}Hg, 0.502 for ^{200}Hg, and 0.752 for ^{201}Hg, to describe the MIF of these three isotopes. The kinetic fractionation factors ($\alpha^{xxx/198}$) were estimated by Rayleigh distillation in a closed system to describe an irreversible sink of pseudo-first kinetic order $R^{xxx}/^{198} = R_0^{xxx/198}\cdot f_R^{(\alpha^{xxx/198}-1)}$, where R and R_0 are ^{xxx}Hg/^{198}Hg ratios for the residual and initial Hg^{II}, respectively, and α is the ratio of the heavy-to-light isotope reduction rates. Introducing the δ-notation, this equation can be approximated by

$$\ln\frac{1000 + \delta^{xxx}\mathrm{Hg}}{1000 + (\delta^{xxx}\mathrm{Hg})_0} = (\alpha^{xxx/198} - 1)\ln(f_R) \quad (1)$$

where $(\delta^{xxx}\mathrm{Hg})_0$ is the initial δ^{xxx}Hg value of the reactant Hg^{II} and the slope represents $\alpha^{xxx/198} - 1$ (units per mille). In turn, the isotope enrichment factor $\varepsilon^{xxx/198}$ is related to $\alpha^{xxx/198}$ by $1000 \times (\alpha^{xxx/198} - 1)$. $\varepsilon^{199/198}$ (units per mille) caused by MIF was derived from the slope of a plot of $\Delta^{199}Hg^{II}-(\Delta^{199}Hg^{II})_0$ versus $\ln(f_R)$, where $(\Delta^{199}\mathrm{Hg})_0$ is the initial $\Delta^{199}Hg^{II}$ value.[35] Linear regressions of Δ^{199}Hg versus Δ^{201}Hg for the different reductants were conducted by the York method using the IsoplotR[36] package on R version 4.0.4.[37]

Instrumental mass bias correction was achieved using Tl (NIST SRM 997) as an internal standard and external standard-sample bracketing with a NIST SRM 3133 Hg solution. A typical sequence consisted of measuring the NIST-3133 Hg standard before and after each sample. The acid and Hg concentrations of the bracketing solution were systematically adjusted to within 10% of the sample. On-peak-zero mode was used during all measurements. The long-term reproducibility of the isotope measurements was assessed by repeated measurements of secondary standard solutions NIST 3177, UM-Almaden, and IGCAS Fluka relative to NIST-3133 (Table S4).

RESULTS AND DISCUSSION

Reaction between Oxalic Acid and Divalent Hg. Despite claims of the existence of $\{Hg(C_2O_4)_2\}^{2-}$,[38] the only aquatic mercuric complex of oxalate characterized with a stability constant is HgC_2O_4 (K_s = 4.6 × 10^9 M^{-1} [39]). By operating at low Hg and total oxalate concentrations, Hg^{2+} complexation with HO^- ($\log\beta_2$ = 21.4[32]) become dominant at pH 6.5 (Figure S3). Although not established for oxalate, strong mercuric hydroxyl carboxylate complexes are recorded for a series of multi-carboxylic acids.[40] The reactivity of these compounds is unknown but previous laboratory experiments show that neutral $Hg(OH)_2$ can be slowly photo-decomposed into Hg^0 by sunlight.[41] Consequently, all experiments were carried out at pH ≤ 5.5 characteristic of atmospheric waters. In all cases, insignificant production of Hg^0 occurred in the blank or dark control experiments (Figure S1). Given the excess of oxalic acid in the experiments, pseudo-first-order kinetics was obtained for the other reactant Hg^{II}. When the recovery was approximately unity, $-\mathrm{d}[Hg^{II}]/\mathrm{d}t \cong \mathrm{d}[Hg^0]/\mathrm{d}t$ allowing us to conveniently follow the course of the reaction by detecting the evolution of the volatile product Hg^0 according to

$$\ln([Hg^{II}]_{t=0}/([Hg^{II}]_{t=0} - [Hg^0]_t)) = k_{obs}\bullet t \quad (2)$$

where k_{obs} is the apparent reaction rate coefficient, t is reaction time, $[Hg^0]$ and $[Hg^{II}]$ represent Hg^0 and Hg^{II} concentrations, respectively. k_{obs} is substantially greater when reaction mixtures are irradiated with UVB compared with UVA radiation (spectral data in Table S1) with a maximum k_{obs} of ∼1.2 × 10^{-3} and ∼0.9 × 10^{-3} s^{-1}, respectively. If normalized to the photon flux, the photo-decomposition frequency is more than quadrupled in UVB compared to UVA light. For actinic light, the absorption of HgC_2O_4 extends into the UVB with weak bands[28] and the photolysis has been described as a reductive elimination in one kinetic step[42−44]

$$HgC_2O_4 \xrightarrow{h\nu} Hg^0 + 2CO_2 \quad (3)$$

https://doi.org/10.1021/acs.est.1c03171
Environ. Sci. Technol. 2021, 55, 13376−13386

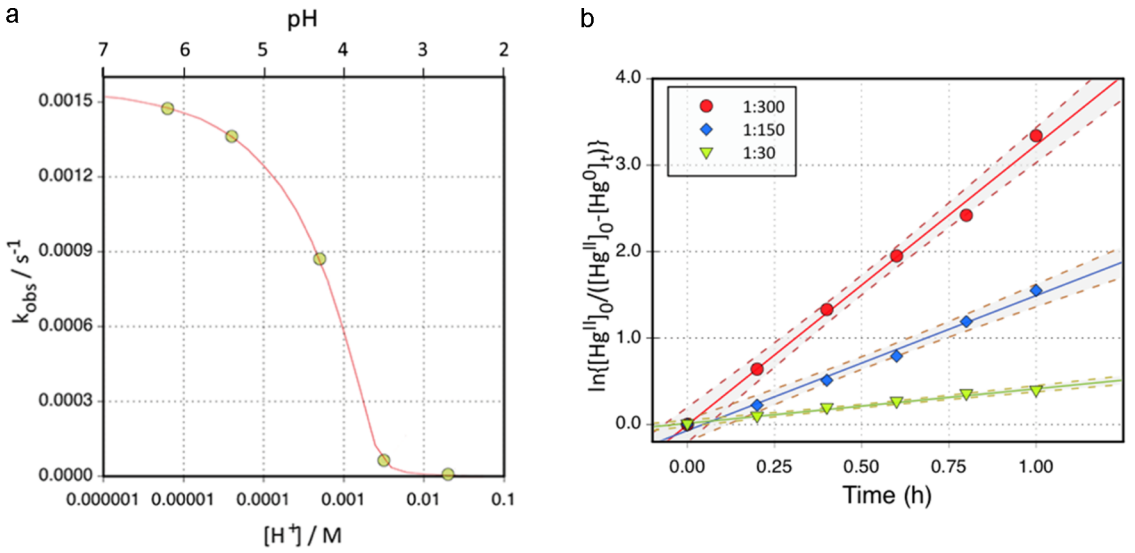

Figure 1. (a) Dependence of the pseudo-first-order rate coefficient for photoreduction of Hg^{II} with $H_2C_2O_4$ on the concentration of hydrogen ion. The solid curve is the fit to eq 5. (b) Reduction of Hg^{II} by various concentrations (0.03, 0.15, and 0.3 mM corresponding to 1:30, 1:150, and 1:300 stoichiometric ratios, respectively) of oxalic acid in excess at pH 3.6.

As expected from actinometric studies,[45] the rate of aqueous HgC_2O_4 photolysis is found to be temperature-dependent. The effect of temperature was studied over the narrow range between 295 and 303 K over which k_{obs} was observed to increase from 1.3 to 2.4 × 10^{-3} s^{-1} corresponding roughly to a doubling of the rate for each 10° increase.

Dependence of pH and Ligand Concentration. The pseudo-first-order rate constant of eq 2 is greatly pH-dependent and shows an asymptotic behavior towards high pH (Figure 1a). Previous investigations either excluded a pH study[8] or were conducted at disparate pHs (3.9 and 7.0; 5.3 and 12.0, respectively) in that Hg^{2+} speciation is diametrically changed.[7,28] In the present study, the course of the pH dependence of k_{obs} suggests that the reactant is the fully deprotonated form of oxalic acid

$$H_2C_2O_4 \rightleftarrows 2H^+ + C_2O_4^{2-}\ K_{a1},\ K_{a2} \tag{4}$$

and

$$k_{obs} = k'\cdot K_{a1}\cdot K_{a2}/([H^+]^2 + K_{a1}\cdot[H^+] + K_{a1}\cdot K_{a2}) \tag{5}$$

is the curve-fitting function. In the pH region (<3) with the predominance of either $HC_2O_4^-$ or $C_2O_4^{2-}$, k_{obs} is largely diminished, indicating that these species are essentially unreactive. The fit to eq 5 yields the intrinsic rate constant k' = 1.8 × 10^{-3} s^{-1} and the acid dissociation constants K_{a1} = 7 × 10^{-2} M^{-1} and K_{a2} = 9 × 10^{-5} M^{-1}. The latter two fitted values compare quite favorably with literature data on oxalic acid at a low ionic strength of pK_{a1} = 1.25 and pK_{a2} = 4.27.[39]

The reaction order was evaluated by varying the oxalic concentration at a fixed pH and initial Hg^{II} concentration. For the oxalic acid concentrations investigated, Figure 1b depicts the course of Hg^{II} decline presented in the logarithmic format of eq 2 plotted as a function of the UVB irradiation time. Analogous to pseudo-first-order plots of the pH effect experiment, the data sets of Figure 1b align well with linear fits. The magnitude of the slopes increase with oxalic acid concentration as a characteristic of a second-order reaction. As previously elucidated here, only the oxalate ion induces Hg^{II} reduction during UV irradiation, and consequently, a bimolecular rate coefficient (k) is formulated as $k = k_{obs}/[C_2O_4^{2-}]$. From the fitted values of k_{obs}, we calculate k to be 15.7 ± 2.8 M^{-1} s^{-1} at 295 ± 1 K. The given error limits include both 10% from systematic experimental error and the 95% confidence interval obtained from least-squares fitting.

Earlier kinetic studies at low concentration level unanimously present evidence that the photochemical reduction of Hg^{II} complexed by oxalate may be of major importance in an atmospheric environment.[7,8,28] Nonetheless, they report conflicting kinetic and mechanistic outcomes. Pehkonen and Lin[7] proposed a secondary two-step $HO_2^\bullet/O_2^{\bullet-}$ reduction mechanism based on photolysis of oxalate in the presence of O_2 (aq)

$$C_2O_4^{2-} + 2O_2 \xrightarrow{h\nu} 2CO_2 + 2O_2^{\bullet-}\ \text{and} O_2^{\bullet-} + H^+ \rightleftarrows HO_2^\bullet\ (pK_a = 4.8) \tag{6}$$

$$Hg^{II} \xrightarrow{HO_2^\bullet/O_2^{\bullet-}} Hg^{I} \xrightarrow{HO_2^\bullet/O_2^{\bullet-}} Hg^0 \tag{7}$$

Using similar reactant concentrations and UV photon fluxes to the present study, the bimolecular rate coefficient of the left-hand step of reaction 7 was estimated by independent methods to be ∼5 × 10^3 ($O_2^\bullet$)[28] and 1.7 × 10^4 ($HO_2^\bullet$)[7] M^{-1} s^{-1}, respectively. From reduction potential measurements, Gårdfeldt and Jonsson[28] rendered under oxic conditions the right-hand step of reaction 7 nullified and suggested that reaction 3 in lieu may help to explain the observed Hg^0 production. A study conducted at pH 3 using part-per-trillion-level Hg^{II} (∼10 ng L^{-1}) irradiated with UV (290−400 nm) yielded a bimolecular rate coefficient between Hg^{II} and total oxalic acid of 1.2 × 10^4 M^{-1} s^{-1}.[8] In retrospect, the magnitude of the reported rate parameter is surprisingly high, as it is on par with that between Hg^{II} and the radicals of reaction 7. Besides, it is obtained for a low pH with the predominance of unreactive protonated forms of oxalate. If erroneously expressed as a function of the total oxalic acid, in comparison, our rate parameter amounts to roughly 1.3‰ of their value. Given the low Hg quantity investigated (∼1 ng Hg) and their large excess of UV photolabile nitrate, we argue that experimental

https://doi.org/10.1021/acs.est.1c03171
Environ. Sci. Technol. 2021, 55, 13376−13386

peculiarities of Si and Ariya[8] made it difficult to curtail the spurious Hg loss that ubiquitously occurs in waters containing ultra-trace Hg concentrations.[29]

Mechanism. The photoreduction of Hg^{II} complexed by oxalate is retarded by dissolved O_2 (Table S6),[28,45] as well as by competitive complexing ligands such as Cl^-.[28] Since oxalic acid/oxalate does not discernibly photo-decompose by actinic radiation,[46] the information gathered above suggests that the photoreduction of Hg^{II} occurs initially via excited HgC_2O_4 (η^2-oxalate) states that decompose in a branched way. The formation of Hg^0 takes place partly by heterolytic reductive elimination (reaction 3) of oxalate promptly to two CO_2, which is relatively unaffected by the presence of radicals, ions, and scavengers (Figure S6) and partly by homolysis of an Hg–O bond, which starts a chain reaction (Figure S5). The photoinduced homolysis is as follows

$$HgC_2O_4 + h\nu \rightleftarrows [Hg\cdots C_2O_4]^* \rightarrow Hg^{\bullet+} + C_2O_4^{\bullet-} \quad (8)$$

where the excited state with radical pair formation is indicated as the intermediate. Formation of Hg^0 would occur from the thermal reaction between $Hg^{\bullet+}$ and the bulk ligand[8]

$$Hg^{\bullet+} + C_2O_4^{2-} \rightarrow Hg^0 + C_2O_4^{\bullet-} \quad (9)$$

$Hg^{\bullet+}$ is reformed from free Hg^{2+} in solution by the action of oxalyl ($C_2O_4^{\bullet-}$) and the carbon dioxide anion radical ($CO_2^{\bullet-}$)

$$Hg^{2+} + C_2O_4^{\bullet-} \rightarrow Hg^{\bullet+} + 2CO_2 \quad (10)$$

$$Hg^{2+} + CO_2^{\bullet-} \rightarrow Hg^{\bullet+} + CO_2 \quad (11)$$

Formed by rapid decarboxylation of $C_2O_4^{\bullet-}$ ($C_2O_4^{\bullet-} \rightarrow CO_2^{\bullet-} + CO_2$, $k = 2 \times 10^6$ s^{-1} [47]), $CO_2^{\bullet-}$ is in comparison the stronger reductant for Hg^{II} with $k_{10} = 5.9 \times 10^8$ M^{-1} s^{-1}.[48] In the presence of dissolved O_2, Hg^{2+} must compete with O_2 for $CO_2^{\bullet-}$ ($CO_2^{\bullet-} + O_2 \rightarrow O_2^{\bullet-} + CO_2$, $k = 2.4 \times 10^9$ M^{-1} s^{-1} [49]). Besides, $Hg^{\bullet+}$ is efficiently re-oxidized to Hg^{2+} by O_2 ($Hg^{\bullet+} + O_2 \rightarrow O_2^{\bullet-} + Hg^{2+}$, $k \geq 1 \times 10^9$ M^{-1} s^{-1} [30]). Consequently, the production of Hg^0 is limited in the presence of O_2 (Figure S6).[8] Experiments conducted in a 1% O_2 mixture in Ar at pH 3.9 yielded a k_{obs} that is ~6% of the magnitude observed under anoxic conditions (Table S6). The branching ratio k_3/k_8, i.e., the fraction of HgC_2O_4 that undergoes reductive elimination to the fraction that is decomposed, initiated by a 1e-LMCT mechanism, is challenging to examine (cf. Figure S5). However, since reaction 8 proceeds by a radical pair mechanism, it is likely to trigger a large degree of odd-MIF in contrast to reaction 3. The observation of odd-MIF is accounted for in the section "Hg Stable Isotope Fractionation during Various HgII Reduction Experiments".

Reaction between *p*-Quinones/Quinol and Divalent Hg. Hg^{II} interacts with *ortho*-QH_2 moieties such as those in natural polyphenols of humic substances and tannins.[50] A direct reaction yields redox-active Hg complexes with ligands of semiquinone radical character that eventually may decompose into Hg^0.[51] The formation as well as structure of Hg–semiquinone complexes is pH-dependent.[51] However, the coordination chemistry of Q/QH_2 species with Hg^{II} has been sparsely documented, with the accounts almost exclusively dealing with *ortho*-QH_2.[51,52,51,52] To the best of our knowledge, no mercuric complexes of para-species have been characterized with a stability constant. We studied the simplest para-substituted Q/QH_2, namely BQ, BQH_2, and AQDS, mimicking polycyclic organic matter (POM) identified in the atmosphere.[53] All of these compounds absorb actinic light substantially, especially in the UV part, and the photoreduction of the Q species is rather efficient.[54] Unlike the other compounds, BQH_2 discernibly reacts with Hg^{II} in the dark, yielding Hg^0 and BQ as end products[14]

$$Hg^{2+} + C_6H_4(OH)_2 \rightarrow C_6H_4(=O)_2 + Hg^0 + 2H^+ \quad (12)$$

As depicted in Figure 2, the observed rate coefficient for the dark reaction is calculated to be $(8.2 \pm 2.4) \times 10^{-5}$ s^{-1}.

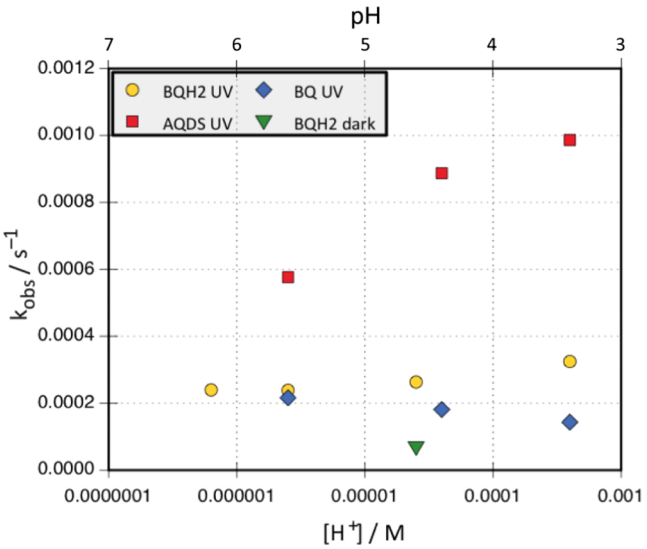

Figure 2. Dependence of the pseudo-first-order rate coefficient for UV photoreduction of Hg^{II} (~1 μM) with BQH_2, BQ, and AQDS (~0.3 mM) on the concentration of hydrogen ion. Inserted is also k_{obs} for the dark reduction between Hg^{II} and BQH_2 measured at pH 4.6 (green triangle). Detailed data are provided in Table S7.

Also shown in Figure 2, k_{obs} shows disparate pH dependence for the UV photoreduction of Hg^{II} by the different Q/QH_2 that plausibly reflect a Hg^{II} ligation effect.[55] For all pHs, the investigated k_{obs} increases in the order BQ, BQH_2, and AQDS. For AQDS, k_{obs} attains at pH 3.4 a maximum value similar to that of the oxalate reaction (cf. Figure 1a). Below pH ~ 5, the rate of photoreduction by BQH_2 increases with $[H^+]$ from an apparent leveling-off section at higher pH. The ligation of Hg^{II} is dominated by $Hg(OH)_2$ (~98%) at pH 4.6 and beyond, while at pH 3.4, the proportions of both Hg^{2+} (16.8%) and $HgOH^+$ (16.8%) gain importance (Table S5, reaction 13).

$$Hg^{2+} + nH_2O \rightleftarrows \{Hg(OH)_n\}^{(2-n)+} + nH^+ \quad (13)$$

"Free" Hg^{2+} and $HgOH^+$ are more reactive than $Hg(OH)_2$, as one may expect[56] when interacting with the quinol. The mechanism of reaction 12 has been elucidated, involving the formation of a phenoxymercury species (reaction 14) followed by 2e-LMCT (reaction 15) rather than an ipso-mercuration mechanism (outlined in Figure S7).[14] There is nothing in our data to contradict that this is also the case for photoreduction of Hg^{II}

$$\{Hg(OH)_n\}^{(2-n)+} + C_6H_4(OH)_2 \rightleftarrows \{(HO)_{n-1}-Hg-OC_6H_4OH\}^{(2-n)+} + H_2O \quad (14)$$

https://doi.org/10.1021/acs.est.1c03171
Environ. Sci. Technol. 2021, 55, 13376–13386

Table 1. k_{obs} with 95% Confidence Intervals and 5% Systematic Errors (Isotopic Parameters Given within 95% Confidence Intervals)[a]

reductant	conditions	k_{obs} (s^{-1})	ε^{202} (‰)	ε^{199} (‰)	$\alpha^{202/198}$
BQH2	dark, pH 4.6	$(8.2 \pm 2.4) \times 10^{-5}$	-1.25 ± 0.19	0.12 ± 0.07	0.99875
BQH2	UVB, pH 3.4	$(3.2 \pm 0.5) \times 10^{-4}$	-1.36 ± 0.12	0.07 ± 0.06	0.99864
BQ	UVB, pH 5.6	$(2.2 \pm 0.4) \times 10^{-4}$	-1.11 ± 0.06	0.05 ± 0.06	0.99889
AQDS	UVB, pH 3.4	$(9.9 \pm 2.7) \times 10^{-4}$	-0.66 ± 0.10	-0.86 ± 0.09	0.99934
$C_2O_4^{2-}$	UVB, pH 3.9 and 5.2	$(9.3 \pm 1.6) \times 10^{-4}$	-1.45 ± 0.06	0.15 ± 0.03	0.99841

[a]For oxalate, the reported kinetics is based on the average of anoxic data at two pH values, and ε^{202}, ε^{199}, and $\alpha^{202/198}$ are the averages for both oxic and anoxic experiments.

$$\{(HO)_{n-1}-Hg-OC_6H_4OH\}^{(2-n)+} \xrightarrow{h\nu/\Delta} C_6H_4(=O)_2 + Hg^0 + H^+(n=1)/H_2O(n=2) \quad (15)$$

The reductive elimination mechanism of reaction 15 outlined in Figure S7 is supported by the isotopic composition measurements, which give a low degree of odd-MIF during dark and UV irradiation (section "Hg Stable Isotope Fractionation during Various HgII Reduction Experiments"). The aqueous photochemistry of quinones is complicated and may involve both ground- and excited-state reactions as well as free radicals.[54] The absorption spectrum of BQ has a maximum in UVC, but extends to the visible light ($\varepsilon_{240} = 2 \times 10^4$ M^{-1} cm^{-1} and $\varepsilon_{440} = 200$ M^{-1} cm^{-1}).[54,57] Following von Sonntag et al.,[57] the reaction scheme of Figure S7 shows that the photoreduction of BQ produces equal amounts of BQH_2 and 2-BQOH. Superimposed in the scheme are the Hg reactions we envisage to be involved. Analogous to BQH_2, BQ is found to photoreduce Hg^{II} in UVB, with a mutually similar reaction frequency at pH 5.6 ($\sim 2.2 \times 10^{-4}$ s^{-1}, Figure 2). It is conceivable to assume that BQH_2, as the photoproduct, also in this case drives the Hg^0 production. However, $k_{obs}(Hg^{II} + BQ + UVB)$ declines with $[H^+]$ in contrast to $k_{obs}(Hg^{II} + BQH_2 + UVB)$, and the ratio $k_{obs}(Hg^{II} + BQH_2 + UVB)/k_{obs}(Hg^{II} + BQ + UVB)$ grows from unity to a value of ~2.3 at pH 3.4. This divergent behavior is difficult to interpret, but may be related to a lower production of BQH_2 from BQ or increased presence of oxidizing radicals (e.g., $^{\bullet}OH$) at low pH.[54]

AQDS is an effective electron shuttle[58] that facilitates electron transfer from metal-reducing bacteria (MRB) to Hg^{II},[59] as well from Hg^0 (aq) to organic thiols (R-SH) during oxidative complexation, forming $Hg(SR)_2$.[12] Zheng et al.[12] reported that AQDS (aq) individually during dark and anaerobic conditions is capable of neither oxidizing Hg^0 nor reducing Hg^{II} (cf. Figure S1). AQDS-assisted biotic Hg^{II} reduction by the MRB Shewanella oneidensis MR-1 is associated with the scavenging of negative charge that temporarily increases the content of reduced AQDS species, such as AQH_2DS and semiquinone radicals, in the system.[59] Alone, the anthraquinol species AQH_2DS is a potent reductant of Hg^{II} in the dark[60] and most plausibly also in actinic light, while the action of AQDS on Hg^{II} in irradiated aqueous solutions was investigated here for the first time. As shown in Figure 2, UVB-irradiated AQDS (aq) is an effective reductant of Hg^{II}. In the UVA photolysis of NQ with an excess of Hg^{II} and HCOOH at pH < 2, Berkovic et al.[15] reported that, in their system, a reaction between Hg^{II} and NQ compared to reaction 10 was insignificant. $k_{obs}(Hg^{II} + AQDS + UVB)$ is on par with that of the oxalate reaction ($\sim 1 \times 10^{-3}$ s^{-1}) as aforementioned, and nearly 7-fold larger than that of Hg^{II} + BQ at the lower end of the pH range investigated. The Hg^{II} + AQDS reaction shows an opposite yet stronger pH dependence in comparison to the Hg^{II} + BQ-irradiated system. As outlined in Figure S8, the reduction of Hg^{II} is mediated via the formation of a chelated structure with $AQH_2(OH)DS$, the photohydrated product of AQDS. The complex of the radical pair (Hg^{I}–semiquinone) character[50] makes the O-bonded $Hg^{\bullet+}$ ($RO-Hg^{\bullet+}$) susceptible to further reduction to Hg^0, which splits away. The pH dependence can be rationalized by the hydrolysis of Hg^{2+} (reaction 13), which causes the reduction to slow down at low $[H^+]$. Admission of O_2 to the solution causes the photoreduction of Hg^{II} to experience a substantial slowdown (Table S6). This behavior can be explained by the triplet AQDS quenching and scavenging of $RO-Hg^{\bullet+}$ by O_2, which are two processes that work together to suppress Hg^0 production.

Hg Stable Isotope Fractionation during Various Hg^{II} Reduction Experiments. *Mass-Dependent Fractionation.* In Table 1, kinetic MDF fractionation factors $\alpha^{202/198}$ are listed for the studied reactions under the given experimental details. They are calculated using a linear regression of eq 1 (plotted in Figure S4) on the measurements of the reactant pool (Table S8). In all cases, when Hg^{II} is reduced in our experiments, a normal kinetic isotope effect (KIE) results in a faster removal of lighter isotopes in the reactant ($\alpha^{202/198} < 1$). Our measured $\alpha^{202/198}$ value falling in the range from 0.99841 to 0.9934 (corresponding to the ε^{202} ranging from −1.45 to −0.66, Table 1) compares well with those of experimental abiotic Hg^{II} photoreduction reported in the literature.[23] In our investigation, due to its small absolute value, ε^{202} for AQDS differs from that of the other compounds, indicating less extensive MDF during this reaction. Nonetheless, the value (-0.66 ± 0.10) is comparable with that reported for actinic light Hg^{II} reduction by fulvic acid (FA; ~−0.6) in the seminal paper of Bergquist and Blum.[61] By using a high ratio of Hg to FA (≥60 μg mg^{-1})[61] in their experiments, they forced Hg^{II} to bind predominantly to hard donor groups (O/N-containing) instead of soft donor ones (S-containing).[62,63] Through a large element of aromatic substances (25−30%) and low N content,[64] it could be speculated that the photochemistry of the conditional Hg^{II}–O binding environment in the FA experiment has significant similarities to our AQDS experiment.

Mass-Independent Fractionation. Displaying a low extent of MDF, in this study, the photoreduction of Hg^{II} by AQDS resulted in a very large magnitude of odd-MIF, with maximum values of $\Delta^{199}Hg$ and $\Delta^{201}Hg$ exceeding 2.5‰ in the reactant pool ($\varepsilon^{199} = -0.86 \pm 0.09$‰). As also shown in Figure 3, the product Hg^0 displays a reciprocal negative magnitude of $\Delta^{199}Hg$ and $\Delta^{201}Hg$ values. Moreover, in all cases, each of the reactant and product samples displays nearly equal odd-MIF signatures ($\Delta^{199}Hg \approx \Delta^{201}Hg$). Finally, no significant MIF of

https://doi.org/10.1021/acs.est.1c03171
Environ. Sci. Technol. 2021, 55, 13376−13386

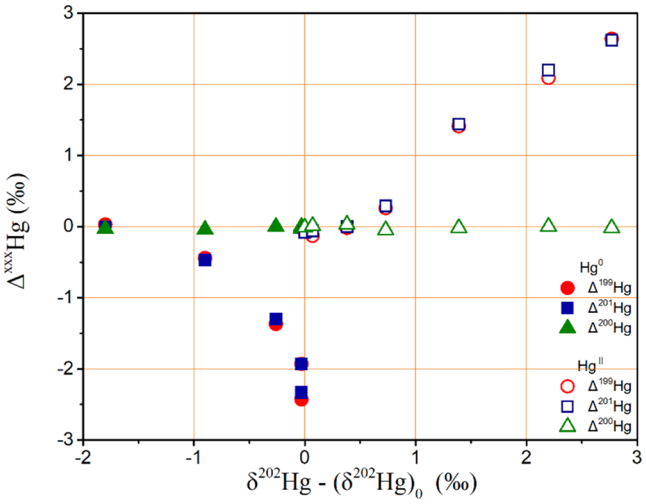

Figure 3. Scatterplot of Δ^{xxx}Hg (*xxx* = 199, 200, and 201) versus δ^{202}Hg for UVB photoreduction of Hg^{II} at pH 3.4 mediated by AQDS. Open markers are samples of reactant Hg^{II} and filled ones are samples from the product Hg^0 during the reaction course. $(\delta^{202}Hg)_0$ represents the initial composition of Hg^{II} in the reaction mixture.

even isotopes is triggered in any of the reduction experiments (Δ^{200}Hg values are within the analytical precision reported in Table S4). Our range of odd-MIF observations, the ratio $\Delta^{199}Hg/\Delta^{201}Hg$ of unity (Figure 4a), and, as aforementioned, $\varepsilon^{202} = -0.66 \pm 0.10$ are all very similar to the isotopic results for Hg^{II} reduction by FA in full sunlight,[61] but to a lesser extent similar to those in light filtered from UVB.[65] Photoreduction by water bulk NOM studied for lower Hg^{II} concentration ratios ($\leq$8.33 μg mg^{-1}) shows in comparison deviations in the reaction rate, kinetics, and isotope fractionation. Both the degree of odd-MIF and the ratio $\Delta^{199}Hg/\Delta^{201}Hg$ are affected by the ratio between Hg^{II} and bulk NOM, where the latter well exceeds unity (1.19−1.31 for photoreduction and ∼1.54 for reduction in the dark).[63] For humic substances, the mechanism connected with the Hg^{II} photoreduction has been suggested to involve $Hg^{\bullet+}$ (FA[61]) and a 1e$^-$-LMCT-type reaction, schematically written as $R{-}Hg^{II} + h\nu \rightarrow R^{\bullet} + H^{I}$ (bulk NOM[63]). Hg^I (representing $Hg^{\bullet+}$ or Hg_2^{2+}) is, according to Zheng and Hintelmann,[63] quickly reduced to Hg^0 in the presence of an excess of electron donors (e.g., organic compounds). However, in our experiment, the abundance of free aqueous $Hg^{\bullet+}$ is unfeasible since the parent molecule AQDS may efficiently re-oxidize it[66]

$$Hg^{\bullet+} + AQDS \rightarrow Hg^{2+} + AQ\bullet - DS \quad (16)$$

where $AQ^{\bullet-}$ DS is the semiquinone anion radical analogue of AQDS. In Figure S8, details of the actinic light photolysis of dilute aqueous AQDS solutions are outlined, following Garg et al.[67] The major photoproduct is a hydroxy-anthraquinol ($AQH_2(OH)DS$). Multifrequency electron spin resonance (ESR) spectroscopic studies of the interaction between Hg^{II} and various humic-like polyphenols have revealed that a prerequisite for the formation of Hg^I−semiquinone complexes is the presence of two vicinal hydroxyl groups at the phenyl ring.[50] Although not specifically studied before, $AQH_2(OH)$-DS fulfills this criterion and is expected to form a chelating binding mode with Hg^{2+} as depicted in Figure S8. The directions of odd-MIF (+MIE) observed in the reactant and product pool of the UVB-illuminated Hg^{2+} + AQDS system (Figure 3) corroborate that 1e-LMCT occurs in an excited AQH(OHg)DS chelate with a radical pair resulting, which is most likely but not necessarily born in a triplet state.[22] As detailed in Figure S9, the overall spin of the triplet radical pair can be changed (intersystem crossing, ISC) in the presence of the magnetic ^{199}Hg and ^{201}Hg by the hyperfine coupling mechanism (HFC). The formed singlet radical pair enriched in odd Hg isotopes recombines to remake the photolyzed bond by its paired electrons, leading back to the ground-state chelate. In contrast, recombination of the triplet radical pair is spin-forbidden, and when the pair separates, $RO{-}Hg^{\bullet+}$ becomes available for reduction tentatively by $AQH_2(OH)DS$, leading to volatile Hg^0 being split off (Figure S9). The large magnitude of odd-MIF imparted indicates an efficient ISC between the radical pairs, which is supported by the larger HFC constants for mercurous radicals with ionic character.[68]

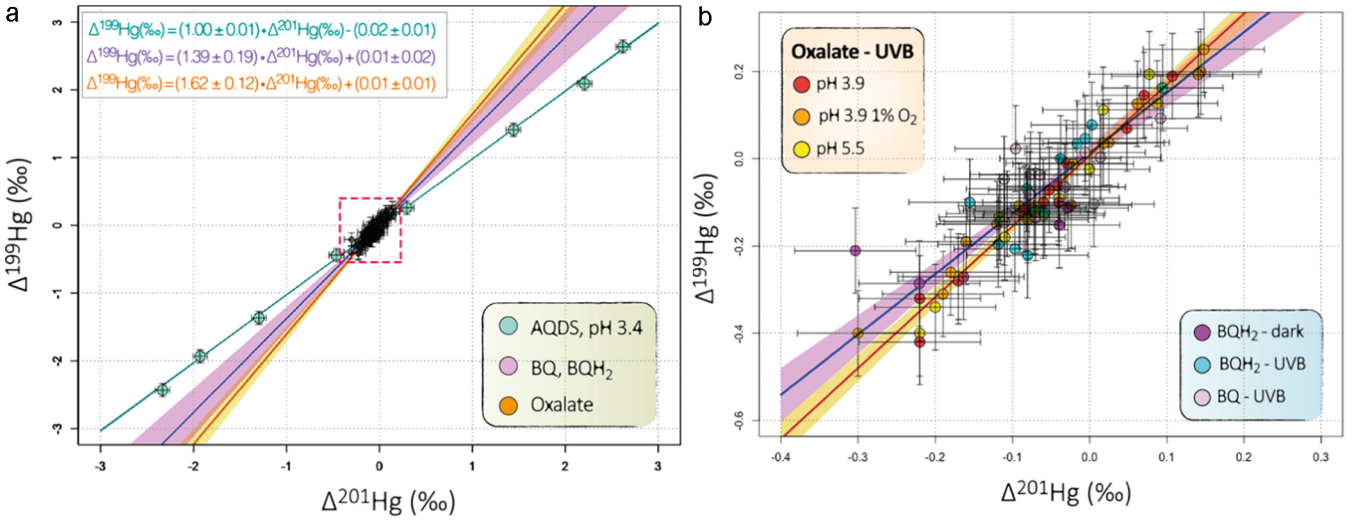

Figure 4. (a) Scatterplot of $\Delta^{199}Hg/\Delta^{201}Hg$ in the reactant and product pool during reduction by various compounds. Lines are the corresponding fits from York regression, and envelopes represent 95% confidence intervals of the mean. (The slope and intercept of the lines are given in the upper left corner within one standard deviation ($\pm 1\sigma$).) (b) Magnification of the dashed rectangle in the center of the left panel. Error bars represent analytical uncertainties ($\pm 3\sigma$, Table S4).

https://doi.org/10.1021/acs.est.1c03171
Environ. Sci. Technol. 2021, 55, 13376−13386

In turn, the decrease in Hg^0 production in the oxic environment (Table S6) is due to a number of interacting factors, as indicated in Figure S8: trapping of mercurous radicals ($RO-Hg^{\bullet+}$) and excited triplets of AQDS, as well as of AQH(OHg)DS by ground-state dissolved O_2.

The other studied organic reducing agents give rise to a comparatively low level of ε^{199}, which also has the opposite sign vis-à-vis ε^{199} for AQDS + UVB (Table 1). The negative $\Delta^{199}Hg$ and $\Delta^{201}Hg$ but positive $\delta^{199}Hg$ and $\delta^{201}Hg$ unanimously characterize the remaining Hg^{II} pool (Table S8). We have performed most isotope analyses on the UVB-irradiated $Hg^{II} + C_2O_4^{2-}$ system, which includes a range of pH and oxic as well as anoxic conditions. Mutually, these $Hg^{II} + C_2O_4^{2-}$ data sets obtained at different reaction conditions present similar distribution and slope in the $\Delta^{199}Hg-\Delta^{201}Hg$ space (Figure 4b). Linear regression of all data gives a slope of 1.62 ± 0.12 (Figure 4a), which falls within the range 1.54−1.66 determined for processes that have been attributed to NVE in the literature.[13] In the context of previous LMWOC studies (stoichiometric ratio $LMWOC/Hg^{II} \geq 2000$), our $Hg^{II} + C_2O_4^{2-}$ isotope data are similar to those reported for UV photolysis of mercuric serinate complexes specifically during its initial phase, but not for further advanced reduction approaching completion.[35,69] In our case, both ε^{202} and ε^{199} are quite constant over the entire reduction process ($f_R > 0.01$), which well follows the Rayleigh fractionation model (eq 1), while both Zheng and Hintelmann[69] and Motta et al.[35] observed for serine (anoxic, pH 3.8) an abrupt shift from weak-negative (NVE) to strong-positive odd-MIF (+MIE and NVE) in the remaining Hg^{II} for an advanced extent of photoreduction. Motta et al.[35] report the emergence of +MIE already when more than 20% of Hg^{II} is remaining, and that the onset coincides with MDF being strongly suppressed ($\varepsilon^{MDF} \sim 0.05‰$). From a single screening experiment (anoxic, pH 6) for a series of LMWOC including both serine and oxalic acid, the onset of +MIE appears near complete UV−vis Hg^{II} photoreduction ($f_R = 0.11$) by $C_2O_4^{2-}$.[69] A shift in dominant isotope effect has been interpreted as a transition from a prevailing secondary to a primary reduction mechanism.[35,69] Without clearly considering the plausibility, the initial reduction phase associated with NVE has been supposed to occur bimolecularly with free radicals.[69] However, since neither oxalic acid nor serine (HSer) absorb sunlight, the corresponding mercuric carboxylate complexes are the only species that may generate free radicals upon irradiation. The net Hg^0 production in the serine experiments may be explained as a result of the reductive elimination with CO_2 and 2-aminoethanol as co-product. Moreover, that the reduction by serine is not suppressed by dissolved O_2,[35] in contrast to that by oxalate, shows that the initial phase may not involve free radicals at all. If radicals were to control the net reduction, one would expect an initial phase with increased Hg^0 production from a low level as it takes time for the radical concentration to build up. The lack of a time lag for serine suggests that NVE arises here through an intramolecular redox mechanism that benefits from the fact that the dominant complex $HgSer_2$ ($\log\beta_2 = 19.1$[70]) can undergo mercuration, forming an intermediate with a photolabile Hg−C bond.[16] For oxalate lacking aliphatic H atoms that can be substituted by mercuration, the photoreduction emanates from HgC_2O_4. In turn, observations of +MIE explicitly mean there is a net Hg^0 production along the pathways originating in a radical pair mechanism (corresponding to reactions 8−11). The explanation for why +MIE first appears near complete Hg^{II} reduction is at least partially because the termination step when Hg^0 splits off (corresponding to reaction 9) is favored by a diminishing concentration ratio between oxidized Hg and the bulk ligand. In view of the above discussion, it is intriguing that, contrary to the literature,[69] we do not observe any traces of triggered +MIE in the oxalate experiments. We have no convincing explanation for this discrepancy, but it should be noted that the oxalate reaction with our default stoichiometry is completed in almost 1 h, while the +MIE observations in the referred serine studies ($\Delta^{199}Hg^{II} > 0.6‰$) occur only after several hours (>4 h) of photoreduction. The conditions at the single +MIE observation for oxalate[69] also differ from ours in terms of reactor material, pH, light spectrum, concentration levels, and stoichiometry between Hg^{II} and the ligand. However, given the observed O_2 sensitivity of the photoreduction and that +MIE has been previously observed, there is little doubt that photolysis of HgC_2O_4 occurs by both homolytic and heterolytic cleavage of an Hg−O bond (Figures S5 and S6) as has previously been deduced.[8]

Compared to oxalate in UVB light, the reduction mediated by BQH_2 in the dark, as well as by BQ and BQH_2 in UVB light, exhibits odd-MIF in a smaller range (Figure 4b). The proportion in NVE can be explained as that its magnitude due to reduction approximately reflects the change in the 6s orbital electron density of Hg, which is larger for stronger and more electron-withdrawing Hg−O bonds in the HgC_2O_4 chelate than for the complexes formed by reaction 14. The definitive determination of the $\Delta^{199}Hg/\Delta^{201}Hg$-slope is here of low diagnostic credibility, as observations are distributed over a scale similar to that of the magnitude of the corresponding analytical uncertainties. Nevertheless, a York regression of these data combined gives a slope of 1.39, which, given the standard error (±0.19), does not exclude the odd-MIF following NVE. In addition to MDF, NVE makes a certain additive contribution to ε^{202},[23] and, in comparison with other processes involving NVE,[23] ε^{202} attains for the aforementioned reduction processes ($-1.45‰ < \varepsilon^{202} < -1.11‰$) similar values. Besides the dark reactions[71,72] and complexation,[73] an exclusively small odd-MIF subject to NVE has been reported for photochemical Hg^{II} reduction with large excess in the organic ligand, such as that induced by UVC light in the %-level of HCOOH at pH < 1,[74] and in serine solution under exclusive visible light.[35] Referred to as an effect essentially of secondary processes,[23] NVE specifically in the $Hg^{II} + BQH_2 +$ UVB system is plausibly triggered by primary photolysis (reaction 15). MIE is not invoked since Hg^0 is produced entirely via reductive elimination, as outlined in Figure S7. We postulate that the same reaction principally yields Hg^0 during UVB photolysis of BQ, where BQH_2 is a major photoproduct.

Environmental Implications. In summary, we have investigated the kinetics, mechanism, and isotope fractionation for mercuric ion reduction to elemental mercury in the aqueous phase by a number of oxygenated LMWOCs. Some of these organic substances have previously been considered important for mercury redox cycling in the environment, and the dicarboxylic acid $H_2C_2O_4$ has been adopted into Hg air-quality models as a reductant.[75] Our re-investigation has shown that only the fully deprotonated form of oxalic acid ($C_2O_4^{2-}$) contributes to the Hg^{II} photoreduction, which, like the determined bimolecular rate constant, differs greatly from what has been reported in the literature.[8] Consequently, the formation of Hg^0 as a result of the photoreduction of mercuric

https://doi.org/10.1021/acs.est.1c03171
Environ. Sci. Technol. 2021, 55, 13376−13386

dicarboxylates in the environment is less important than previously thought. Furthermore, this process does not result in the isotope fractionation observed in the atmosphere, for example, in Hg^{II} in aerosols that have been subjected to photoreduction.[25] On the contrary, aqueous photoexperiments with AQDS produce very similar kinetics and isotope fractionation characteristics as those from Hg^{II} photoreduction by the humic substance FA. The result supports previous suggestions that Hg^{II} photoreduction by NOM is mostly driven by NOM-bound quinonic moieties.[11] While only quinolic compounds can reduce Hg^{II} to Hg^0 in the dark, both the investigated quinones and quinols readily do so upon UV irradiation. The photolysis rate of Hg^{II} with photohydrated AQDS is relatively fast ($\sim 10^{-3}$ s^{-1}), and in addition, a large odd-MIF is triggered during the reaction. The Hg^{II} photoreduction by AQDS also proceeds by a considerable rate (~3% h^{-1} in actinic light at mid-latitude and noon for summer equinox) in oxic waters, implying that atmospheric reduction of Hg^{II} by NOM should be considered as a potentially important source of Hg^0 that helps to mitigate the existing biases in modeling atmospheric Hg deposition. Being an oxidation product of polycyclic aromatic hydrocarbons (PAHs) that in turn are emitted into the atmosphere as byproducts of, e.g., incomplete combustion processes, quinones (of which anthraquinone (AQ) is one of the main components) are often detected in ambient air[76] and omnipresent in SOA of heavy industrialized regions[77,78] at concentrations that are frequently on par with those of the unreacted parent PAHs. In addition to photohydroxylation,[67] heterogeneous OH reaction[79] is a likely major chemical sink for atmospheric AQ that produces hydroxylated species. As we previously reported here, such products mediate photoreduction of Hg^{II}. Recently, combined measurements of the concentrations and stable isotope composition of airborne particle-bound Hg (PBM) have proven valuable in predicting the extent of Hg^{II} photoreduction by a statistically significant anticorrelation between PBM concentration and the corresponding $\Delta^{199}Hg$.[24] Fu et al.[25] found that nearly depleted PBM (<10 pg Hg m^{-3}) has $\Delta^{199}Hg$ values that are up to 1‰ more positive than particles with high Hg content (>50 pg Hg m^{-3}) that are characteristic of primary anthropogenic emissions not processed by Hg^{II} photoreduction. Atmospheric interaction of Hg^{II} with organic aerosols may therefore assist to explain the large $\Delta^{199}Hg$ in particulates of SOA type. At this point, however, a deeper understanding of how key parameters affect the isotope signals resulting from photoreduction is required. Further studies should be concerned with establishing a wider range of reactions at a molecular mechanistic level.

■ ASSOCIATED CONTENT

Supporting Information

The Supporting Information is available free of charge at https://pubs.acs.org/doi/10.1021/acs.est.1c03171.

Complementary materials including details of chemicals and reagents, figures related to e.g. experimental blanks, speciation, isotope fractionation kinetics and mechanism, and tables showing e.g. experimental conditions, QA/QC, kinetics and comprehensive isotopic sample data (PDF)

■ AUTHOR INFORMATION

Corresponding Authors

Bo Meng − *State Key Laboratory of Environmental Geochemistry, Institute of Geochemistry, Chinese Academy of Sciences, Guiyang 550081, China;* orcid.org/0000-0002-7827-8673; Phone: +86-851-84396920; Email: mengbo@vip.skleg.cn; Fax: +86-851-85891721

Xinbin Feng − *State Key Laboratory of Environmental Geochemistry, Institute of Geochemistry, Chinese Academy of Sciences, Guiyang 550081, China; Center for Excellence in Quaternary Science and Global Change, Chinese Academy of Sciences, Xian 710061, China;* orcid.org/0000-0002-7462-8998; Phone: +86-851-85895728; Email: fengxinbin@vip.skleg.cn; Fax: +86-851-85891721

Jonas Sommar − *State Key Laboratory of Environmental Geochemistry, Institute of Geochemistry, Chinese Academy of Sciences, Guiyang 550081, China;* orcid.org/0000-0001-8634-440X; Phone: +86-015885096925; Email: jonas@vip.skleg.cn; Fax: +86-851-85891721

Authors

Huifang Zhao − *State Key Laboratory of Environmental Geochemistry, Institute of Geochemistry, Chinese Academy of Sciences, Guiyang 550081, China; School of Geography & Environmental Science, Guizhou Normal University, Guiyang 550025, China*

Guangyi Sun − *State Key Laboratory of Environmental Geochemistry, Institute of Geochemistry, Chinese Academy of Sciences, Guiyang 550081, China;* orcid.org/0000-0001-8522-7973

Che-Jen Lin − *Center for Advances in Water and Air Quality, Lamar University, Beaumont, Texas 77710, United States*

Complete contact information is available at: https://pubs.acs.org/10.1021/acs.est.1c03171

Notes

The authors declare no competing financial interest.

■ ACKNOWLEDGMENTS

The authors would like to acknowledge the support of the National Natural Science Foundation of China (nos. 41673025, 41931297, and 41907286), CAS "Light of West China" program, and Chinese Academy of Sciences (QYZDJ-SSW-DQC005).

■ REFERENCES

(1) UNEP Minamata Convention on Mercury. http://www.mercuryconvention.org/ (retrieved July 18, 2021).

(2) Sommar, J.; Osterwalder, S.; Zhu, W. Recent advances in understanding and measurement of Hg in the environment: Surface-atmosphere exchange of gaseous elemental mercury (Hg^0). *Sci. Total Environ.* **2020**, *721*, No. 137648.

(3) Blum, J. D.; Sherman, L. S.; Johnson, M. W. Mercury Isotopes in Earth and Environmental Sciences. *Annu. Rev. Earth Planet. Sci.* **2014**, *42*, 249−269.

(4) Åkerblom, S.; Meili, M.; Bishop, K. Organic Matter in Rain: An Overlooked Influence on Mercury Deposition. *Environ. Sci. Technol. Lett.* **2015**, *2*, 128−132.

(5) Lin, C. J.; Pehkonen, S. O. The chemistry of atmospheric mercury: a review. *Atmos. Environ.* **1999**, *33*, 2067−2079.

(6) Alberts, J. J.; Schindler, J. E.; Miller, R. W.; Nutter, D. E. Elemental Mercury Evolution Mediated by Humic Acid. *Science* **1974**, *184*, 895−896.

(7) Pehkonen, S. O.; Lin, C. J. Aqueous photochemistry of mercury with organic acids. *J. Air Waste Manage. Assoc.* **1998**, *48*, 144−150.
(8) Si, L.; Ariya, P. A. Reduction of Oxidized Mercury Species by Dicarboxylic Acids (C_2 - C_4): Kinetic and Product Studies. *Environ. Sci. Technol.* **2008**, *42*, 5150−5155.
(9) Warneck, P. In-cloud chemistry opens pathway to the formation of oxalic acid in the marine atmosphere. *Atmos. Environ.* **2003**, *37*, 2423−2427.
(10) Hallquist, M.; Wenger, J. C.; Baltensperger, U.; Rudich, Y.; Simpson, D.; Claeys, M.; Dommen, J.; Donahue, N. M.; George, C.; Goldstein, A. H.; Hamilton, J. F.; Herrmann, H.; Hoffmann, T.; Iinuma, Y.; Jang, M.; Jenkin, M. E.; Jimenez, J. L.; Kiendler-Scharr, A.; Maenhaut, W.; McFiggans, G.; Mentel, T. F.; Monod, A.; Prévot, A. S. H.; Seinfeld, J. H.; Surratt, J. D.; Szmigielski, R.; Wildt, J. The formation, properties and impact of secondary organic aerosol: Current and emerging issues. *Atmos. Chem. Phys.* **2009**, *9*, 5155−5236.
(11) Zheng, W.; Liang, L. Y.; Gu, B. H. Mercury Reduction and Oxidation by Reduced Natural Organic Matter in Anoxic Environments. *Environ. Sci. Technol.* **2012**, *46*, 292−299.
(12) Zheng, W.; Lin, H.; Mann, B. F.; Liang, L.; Gu, B. Oxidation of Dissolved Elemental Mercury by Thiol Compounds under Anoxic Conditions. *Environ. Sci. Technol.* **2013**, *47*, 12827−12834.
(13) Zheng, W.; Demers, J. D.; Lu, X.; Bergquist, B. A.; Anbar, A. D.; Blum, J. D.; Gu, B. H. Mercury Stable Isotope Fractionation during Abiotic Dark Oxidation in the Presence of Thiols and Natural Organic Matter. *Environ. Sci. Technol.* **2019**, *53*, 1853−1862.
(14) Deacon, G. B.; Odonoghue, F.; McKillop, A.; Young, D. W. Facile oxidations of 1,4-hydroquinones to 1,4-benzoquinones with bromomercury(II) derivatives. *Synth. Commun.* **1980**, *10*, 615−621.
(15) Berkovic, A. M.; Bertolotti, S. G.; Villata, L. S.; Gonzalez, M. C.; Pis Diez, R.; Mártire, D. O. Photoinduced reduction of divalent mercury by quinones in the presence of formic acid under anaerobic conditions. *Chemosphere* **2012**, *89*, 1189−1194.
(16) Horváth, O.; Vogler, A. Photoreduction of mercury(II) in aqueous solution in the presence of cyclohexene. Hydroxomercuration and two-stage photolysis. *Inorg. Chem. Commun.* **1998**, *1*, 270−272.
(17) Roundhill, D. M. *Photochemistry and Photophysics of Metal Complexes*, 1st ed.; Springer US, 1994; p 356.
(18) Mangiante, D. M.; Schaller, R. D.; Zarzycki, P.; Banfield, J. F.; Gilbert, B. Mechanism of Ferric Oxalate Photolysis. *ACS Earth Space Chem.* **2017**, *1*, 270−276.
(19) Brown, S. N.; Mayer, J. M. Photochemical generation of a reactive rhenium(III) oxo complex and its curious mode of cleavage of dioxygen. *Inorg. Chem.* **1992**, *31*, 4091−4100.
(20) Anderson, J. E.; Murphy, C. P.; Real, J.; Balué, J.; Bayón, J. C. Electron transfer properties of rhodium(I) oxalate complexes. *Inorg. Chim. Acta* **1993**, *209*, 151−160.
(21) Van Loon, L. L.; Mader, E. A.; Scott, S. L. Reduction of the aqueous mercuric ion by sulfite: UV spectrum of $HgSO_3$ and its intramolecular redox reaction. *J. Phys. Chem. A* **2000**, *104*, 1621−1626.
(22) Motta, L. C.; Chien, A. D.; Rask, A. E.; Zimmerman, P. M. Mercury Magnetic Isotope Effect: A Plausible Photochemical Mechanism. *J. Phys. Chem. A* **2020**, *124*, 3711−3719.
(23) Hintelmann, H.; Zheng, W. Tracking Geochemical Transformations and Transport of Mercury through Isotope Fractionation. In *Environmental Chemistry and Toxicology of Mercury*; Liu, G.; Cai, Y.; O'Driscoll, N., Eds.; John Wiley & Sons: Hoboken, 2011; pp 293−328.
(24) Huang, Q.; Chen, J.; Huang, W.; Reinfelder, J. R.; Fu, P.; Yuan, S.; Wang, Z.; Yuan, W.; Cai, H.; Ren, H.; Sun, Y.; He, L. Diel variation in mercury stable isotope ratios records photoreduction of PM2.5-bound mercury. *Atmos. Chem. Phys.* **2019**, *19*, 315−325.
(25) Fu, X.; Zhang, H.; Feng, X.; Tan, Q.; Ming, L.; Liu, C.; Zhang, L. Domestic and Transboundary Sources of Atmospheric Particulate Bound Mercury in Remote Areas of China: Evidence from Mercury Isotopes. *Environ. Sci. Technol.* **2019**, *53*, 1947−1957.
(26) Xu, H.; Sonke, J. E.; Guinot, B.; Fu, X.; Sun, R.; Lanzanova, A.; Candaudap, F.; Shen, Z.; Cao, J.-J. Seasonal and annual variations in atmospheric Hg and Pb isotopes in Xi'an, China. *Environ. Sci. Technol.* **2017**, *51*, 3759−3766.
(27) Das, R.; Wang, X.; Khezri, B.; Webster, R. D.; Sikdar, P. K.; Datta, S. Mercury isotopes of atmospheric particle bound mercury for source apportionment study in urban Kolkata, India. *Elementa: Sci. Anthroposphere* **2016**, *4*, No. 000098.
(28) Gårdfeldt, K.; Jonsson, M. Is bimolecular reduction of Hg(II) complexes possible in aqueous systems of environmental importance? *J. Phys. Chem. A* **2003**, *107*, 4478−4482.
(29) Feldman, C. Preservation of dilute mercury solutions. *Anal. Chem.* **1974**, *46*, 99−102.
(30) Gårdfeldt, K.; Sommar, J.; Strömberg, D.; Feng, X. B. Oxidation of atomic mercury by hydroxyl radicals and photoinduced decomposition of methylmercury in the aqueous phase. *Atmos. Environ.* **2001**, *35*, 3039−3047.
(31) Sun, G.; Sommar, J.; Feng, X.; Lin, C.-J.; Ge, M.; Wang, W.; Yin, R.; Fu, X.; Shang, L. Mass-dependent and -independent fractionation of mercury isotope during gas-phase oxidation of elemental mercury vapor by atomic Cl and Br. *Environ. Sci. Technol.* **2016**, *50*, 9232−9241.
(32) Puigdomenech, I. *SPANA and DATABASE (Modified JAVA Versions of Earlier Software MEDUSA, HYDRA and INPUT-SED-PREDOM)* Department of Inorganic Chemistry, Royal Institute of Technology (KTH): Stockholm, Sweden, 2016. https://www.kth.se/che/medusa/downloads-1.386254.
(33) Müller, B.. *ChemEQL v. 3. 2 (A Program to Calculate Chemical Speciation Equilibria, Titrations, Dissolution, Precipitation, Adsorption, Kinetics, pX-pY Diagrams, Solubility Diagrams. Libraries with Complexation Constants)*; Swiss Federal Institute of Aquatic Science and Technology: Kastanienbaum, Switzerland, 2021. http://eawag.ch/en/department/surf/projects/chemeql/.
(34) Blum, J. D.; Bergquist, B. A. Reporting of variations in the natural isotopic composition of mercury. *Anal. Bioanal. Chem.* **2007**, *388*, 353−359.
(35) Motta, L. C.; Kritee, K.; Blum, J. D.; Tsz-Ki Tsui, M.; Reinfelder, J. R. Mercury Isotope Fractionation during the Photochemical Reduction of Hg(II) Coordinated with Organic Ligands. *J. Phys. Chem. A* **2020**, *124*, 2842−2853.
(36) Vermeesch, P. IsoplotR: a free and open toolbox for geochronology. *Geosci. Front.* **2018**, *9*, 1479−1493.
(37) R CoreTeam. *A Language and Environment for Statistical Computing*; R Foundation for Statistical Computing: Vienna, Austria, 2021. https://www.R-project.org/.
(38) Bullock, J. I.; Tuck, D. G. Solvent extraction of anionic sulphato, selenato and oxalato complexes of mercury (II). *J. Inorg. Nucl. Chem.* **1966**, *28*, 1103−1110.
(39) Martell, A.; Smith, R. M. *Critical Stability Constants: Other Organic Ligands*; Springer: New York, NY, 1977; Vol. 3, p 495.
(40) Kornev, V. I.; Kardapol'tsev, A. A. Heteroligand mercury(II) complexes with aspartic, tartaric, and citric acids. *Russ. J. Coord. Chem.* **2008**, *34*, 896−900.
(41) Xiao, Z.; Munthe, J.; Strömberg, D.; Lindqvist, O. Photochemical Behaviour of Inorganic Mercury Compounds in Aqueous Solution. In *Mercury Pollution: Integration and Synthesis*; Watras, C. J.; Huckabee, J. W., Eds.; Lewis Publishers: Boca Raton, FL, 1994; pp 581−594.
(42) de Waal, D. J. A.; van den Burg, J. A. Photochemical Decomposition of Dioxalatomercurate(II). *Suid-Afrikaanse Tydskrif vir Natuurwetenskap en Tegnologie (South African Journal of Science and Technology)* **1969**, *9*, 1−9 (in Afrikaans).
(43) Wang, Z. Eder Reaction. *Comprehensive Organic Name Reactions and Reagents*; John Wiley & Sons Inc., 2010; pp 952−953.
(44) Ababneh, F. A.; Scott, S. L.; Al-Reasi, H. A.; Lean, D. R. S. Photochemical reduction and reoxidation of aqueous mercuric chloride in the presence of ferrioxalate and air. *Sci. Total Environ.* **2006**, *367*, 831−839.

https://doi.org/10.1021/acs.est.1c03171
Environ. Sci. Technol. 2021, 55, 13376−13386

(45) Roseveare, W. E. The X-ray photochemical reaction between potassium oxalate and mercuric chloride. *J. Am. Chem. Soc.* **1930**, *52*, 2612−2619.
(46) Graddon, D. P. The absorption spectra of complex oxalates. *J. Inorg. Nucl. Chem.* **1956**, *3*, 308−322.
(47) Mulazzani, Q. G.; D'Angelantonio, M.; Venturi, M.; Hoffman, M. Z.; Rodgers, M. A. J. Interaction of formate and oxalate ions with radiation-generated radicals in aqueous solution. Methylviologen as a mechanistic probe. *J. Phys. Chem. A* **1986**, *90*, 5347−5352.
(48) Berkovic, A. M.; Gonzalez, M. C.; Russo, N.; Del Carmen Michelini, M.; Diez, R. P.; Mártire, D. O. Reduction of mercury(II) by the carbon dioxide radical anion: A theoretical and experimental investigation. *J. Phys. Chem. A* **2010**, *114*, 12845−12850.
(49) Bielski, B. H. J.; Cabelli, D. E.; Arudi, R. L.; Ross, A. B. Reactivity of HO_2/O_2^- Radicals in Aqueous Solution. *J. Phys. Chem. Ref. Data* **1985**, *14*, 1041−1100.
(50) Jerzykiewicz, M. The effect of Hg(II) ions on the free radicals of humic substances and their model compounds. *Chemosphere* **2013**, *92*, 445−450.
(51) Jerzykiewicz, M.; Witwicki, M.; Jezierska, J. pH-dependent formation of Hg(II)-semiquinone complexes from natural phenols. *Chemosphere* **2015**, *138*, 233−238.
(52) Frank, R. L.; Clark, G. R.; Coker, J. N. Metallic Complexes of 2,5-Dihydroxy-1,4-benzoquinones. *J. Am. Chem. Soc.* **1950**, *72*, 1827−1829.
(53) Finlayson-Pitts, B. J.; Pitts, J. N. *Chemistry of the Upper and Lower Atmosphere: Theory, Experiments and Applications*, 1st ed.; Academic Press: San Diego, CA, 2000.
(54) Görner, H. Quinone Photochemistry. In *CRC Handbook of Organic Photochemistry and Photobiology*, 3rd ed.; Griesbeck, A.; Oelgemöller, M.; Ghetti, F., Eds.; CRC Press, 2019; Vol. *1*, pp 683−714.
(55) Gopinath, E.; Kaaret, T. W.; Bruice, T. C. Mechanism of mercury(II) reductase and the influence of ligation on the reduction of lmercury(II) by a water-soluble 1,5-dihydroflavin. *Proc. Natl. Acad. Sci. U.S.A.* **1989**, *86*, 3041−3044.
(56) Celo, V.; Scott, S. L. Kinetics and mechanism of the mercury(II)-assisted hydrolysis of methyl iodide. *Inorg. Chem.* **2005**, *44*, 2507−2512.
(57) von Sonntag, J.; Mvula, E.; Hildenbrand, K.; von Sonntag, C. Photohydroxylation of 1,4-Benzoquinone in Aqueous Solution Revisited. *Chem. − Eur. J.* **2004**, *10*, 440−451.
(58) Bai, Y.; Mellage, A.; Cirpka, O. A.; Sun, T.; Angenent, L. T.; Haderlein, S. B.; Kappler, A. AQDS and Redox-Active NOM Enables Microbial Fe(III)-Mineral Reduction at cm-Scales. *Environ. Sci. Technol.* **2020**, *54*, 4131−4139.
(59) Lee, S.; Kim, D.-H.; Kim, K.-W. The enhancement and inhibition of mercury reduction by natural organic matter in the presence of Shewanella oneidensis MR-1. *Chemosphere* **2018**, *194*, 515−522.
(60) Zhu, W. In *Terrestrial Organic Matter Discharges Enhance Mercury Reduction and Emission from Anoxic Sediments*, Proceedings of 13th International Conference on Mercury as a Global Pollutant, TO-060, Providence, RI, July 16−21, 2017.
(61) Bergquist, B. A.; Blum, J. D. Mass-dependent and -independent fractionation of Hg isotopes by photoreduction in aquatic systems. *Science* **2007**, *318*, 417−420.
(62) Haitzer, M.; Aiken, G. R.; Ryan, J. N. Binding of Mercury(II) to Dissolved Organic Matter: The Role of the Mercury-to-DOM Concentration Ratio. *Environ. Sci. Technol.* **2002**, *36*, 3564−3570.
(63) Zheng, W.; Hintelmann, H. Mercury isotope fractionation during photoreduction in natural water is controlled by its Hg/DOC ratio. *Geochim. Cosmochim. Acta* **2009**, *73*, 6704−6715.
(64) Averett, R. C.; Leenheer, J. A.; McKnight, D. M.; Thorn, K. A. *Humic Substances in the Suwannee River, Georgia: Interactions, Properties, and Proposed Structures*, Water Supply Paper 2373; U.S. Government Printing Office, 1994.
(65) Rose, C. H.; Ghosh, S.; Blum, J. D.; Bergquist, B. A. Effects of ultraviolet radiation on mercury isotope fractionation during photoreduction for inorganic and organic mercury species. *Chem. Geol.* **2015**, *405*, 102−111.
(66) Jungbluth, H.; Beyrich, J.; Asmus, K. D. Reduction of mercuric halides and pseudohalides in aqueous solution. Formation and some physicochemical properties of HgCl, HgBr, HgI, HgSCN, and HgCN radical molecules. *J. Phys. Chem. A* **1976**, *80*, 1049−1053.
(67) Garg, S.; Rose, A. L.; Waite, T. D. Production of Reactive Oxygen Species on Photolysis of Dilute Aqueous Quinone Solutions. *Photochem. Photobiol.* **2007**, *83*, 904−913.
(68) Karakyriakos, E.; McKinley, A. J. Matrix Isolated $HgCH_3$ Radical: An ESR Investigation. *J. Phys. Chem. A* **2004**, *108*, 4619−4626.
(69) Zheng, W.; Hintelmann, H. Isotope Fractionation of Mercury during Its Photochemical Reduction by Low-Molecular-Weight Organic Compounds. *J. Phys. Chem. A* **2010**, *114*, 4246−4253.
(70) Van Der Linden, W. E.; Beers, C. Determination of composition and stability-constants of complexes of mercury(II) with amino-acids. *Anal. Chim. Acta* **1974**, *68*, 143−154.
(71) Zheng, W.; Hintelmann, H. Nuclear Field Shift Effect in Isotope Fractionation of Mercury during Abiotic Reduction in the Absence of Light. *J. Phys. Chem. A* **2010**, *114*, 4238−4245.
(72) Kritee, K.; Blum, J. D.; Barkay, T. Mercury stable isotope fractionation during reduction of Hg(II) by different microbial pathways. *Environ. Sci. Technol.* **2008**, *42*, 9171−9177.
(73) Wiederhold, J. G.; Cramer, C. J.; Daniel, K.; Infante, I.; Bourdon, B.; Kretzschmar, R. Equilibrium Mercury Isotope Fractionation between Dissolved Hg(II) Species and Thiol-Bound Hg. *Environ. Sci. Technol.* **2010**, *44*, 4191−4197.
(74) Yang, L.; Sturgeon, R. Isotopic fractionation of mercury induced by reduction and ethylation. *Anal. Bioanal. Chem.* **2009**, *393*, 377−385.
(75) Bash, J.; Carlton, A.; Hutzell, W.; Bullock, O., Jr. Regional Air Quality Model Application of the Aqueous-Phase Photo Reduction of Atmospheric Oxidized Mercury by Dicarboxylic Acids. *Atmosphere* **2014**, *5*, 1−15.
(76) Albinet, A.; Leoz-Garziandia, E.; Budzinski, H.; Villenave, E.; Jaffrezo, J. L. Nitrated and oxygenated derivatives of polycyclic aromatic hydrocarbons in the ambient air of two French alpine valleys: Part 1: Concentrations, sources and gas/particle partitioning. *Atmos. Environ.* **2008**, *42*, 43−54.
(77) Wnorowski, A.; Charland, J.-P. Profiling quinones in ambient air samples collected from the Athabasca region (Canada). *Chemosphere* **2017**, *189*, 55−66.
(78) Niu, X.; Ho, S. S. H.; Ho, K. F.; Huang, Y.; Sun, J.; Wang, Q.; Zhou, Y.; Zhao, Z.; Cao, J. Atmospheric levels and cytotoxicity of polycyclic aromatic hydrocarbons and oxygenated-PAHs in PM2.5 in the Beijing-Tianjin-Hebei region. *Environ. Pollut.* **2017**, *231*, 1075−1084.
(79) Miet, K.; Albinet, A.; Budzinski, H.; Villenave, E. Atmospheric reactions of 9,10-anthraquinone. *Chemosphere* **2014**, *107*, 1−6.

https://doi.org/10.1021/acs.est.1c03171
Environ. Sci. Technol. 2021, 55, 13376−13386